Bifurcations of limit-cycle oscillations of a two degree-of-freedom airfoil caused by aerodynamic non-linearities

van Rooij, Anouk; Nitzsche, J.; Dwight, Richard

DOI
10.2514/6.2017-1359

Publication date
2017

Document Version
Accepted author manuscript

Published in
58th AIAA/ASCE/AHS/ASC Structures, Structural Dynamics, and Materials Conference

Citation (APA)
van Rooij, A., Nitzsche, J., & Dwight, R. (2017). Bifurcations of limit-cycle oscillations of a two degree-of-freedom airfoil caused by aerodynamic non-linearities. In *58th AIAA/ASCE/AHS/ASC Structures, Structural Dynamics, and Materials Conference: Grapevine, Texas, USA* Article AIAA 2017-1359 American Institute of Aeronautics and Astronautics Inc. (AIAA). https://doi.org/10.2514/6.2017-1359

This is an Accepted Manuscript of an article published in: 58th AIAA/ASCE/AHS/ASC Structures, Structural Dynamics, and Materials Conference. 9/01/17 - 13/01/17 Grapevine, Texas, USA ISBN: 978-1-62410-453-4
Available online: https://arc.aiaa.org/doi/10.2514/6.2017-1359

Bifurcations of limit-cycle oscillations of a two degree-of-freedom airfoil caused by aerodynamic non-linearities

A. C. L. M. van Rooij* and J. Nitzsche†
German Aerospace Center (DLR), Institute of Aeroelasticity, 37073 Göttingen, Germany
R. P. Dwight‡
Delft University of Technology, Faculty of Aerospace Engineering, 2629 HS Delft, The Netherlands

Flutter is usually predicted using linearised theory. In reality, flutter is always non-linear and might already occur below the linearly predicted flutter boundary. Whether this is the case for limit-cycle oscillations (LCOs) caused by aerodynamic non-linearities is not known, since these LCOs can only be predicted using expensive wind-tunnel tests or coupled Computational Fluid Dynamics (CFD)-Computational Structural Mechanics (CSM) simulations. However, it is important to know whether a sufficiently large disturbance can already cause LCOs below the flutter boundary predicted from linearised theory. Furthermore, since structural properties and the flow conditions will vary, it is necessary to study the resulting variations of the Hopf bifurcation behaviour of the LCO solutions near the flutter point. In this work viscous and inviscid transonic flows are considered. The LCO bifurcation behaviour was found to vary significantly when the uncoupled structural natural frequency ratio and the location of the elastic axis are changed. When the non-linearity is relatively weak, a change in the Hopf bifurcation type might result. A Mach number variation in inviscid flow showed that the effective flutter boundary might significantly deviate from that predicted using linearised theory. For both the structural parameter variations and the Mach number variation, LCOs were observed below the linearly predicted flutter boundary. At the nominal structural parameters, the amplitude-dependent behaviour of the phase of the lift was found to be responsible for the type of bifurcation of the LCO solution that occurs. Inspection of the local force distributions at various pitch amplitudes showed that the motion of the shock wave on the lower surface is responsible for the behaviour of the phase of the lift and hence for the bifurcation behaviour of the LCOs observed in this work.

Nomenclature

$\mathbf{A}$	generalised aerodynamic force matrix
$\mathbf{D}$	damping matrix
$\mathbf{K}$	stiffness matrix
$\mathbf{M}$	mass matrix
Re	Reynolds number
$\vec{\hat{f}}$	complex amplitude vector of the aerodynamic force
$\vec{\hat{x}}$	motion vector
$\vec{f}$	aerodynamic force vector
$\vec{x}$	time-dependent motion vector
b	wing span, m

*PhD Candidate, Aeroelastic Simulation, Bunsenstrasse 10, and AIAA Member.
†Team Leader, Aeroelastic Simulation, Bunsenstrasse 10.
‡Assistant Professor, Aerodynamics, Wind Energy & Propulsion, Kluyverweg 1.

c chord length, m
c_f skin friction coefficient
c_p pressure coefficient
h plunge displacement, m
I_α mass moment of inertia (about the elastic axis), kgm^2
k reduced frequency
K_h plunge spring stiffness, N/m
K_α torsional spring stiffness, Nm/rad
L lift, N
M Mach number
M moment about the quarter-chord point, Nm
m mass, kg
p complex-valued eigenvalue
p pressure, Pa
q dynamic pressure, Pa
S_α static moment (related to the elastic axis), kgm
T temperature, K
t time, s
U velocity, m/s
x_{ea} distance between quarter-chord point and elastic axis, m

Subscripts

∞ freestream condition
f flutter condition
LCO limit-cycle oscillation condition

Conventions

$|\ |$ magnitude
$\bar{}$ mean value

Symbols

α pitch angle, °
δ amplification rate
$\Delta\alpha$ pitch amplitude, °
ω angular frequency, rad/s
ω_h uncoupled natural plunge frequency, rad/s
ω_α uncoupled natural pitch frequency, rad/s
$\phi_{h\alpha}$ phase difference between pitch and plunge, °
ϕ_{Lh} phase of the lift w.r.t. the plunging motion, °
$\phi_{M\alpha}$ phase of the moment w.r.t. the pitching motion, °
ρ density, kg/m^3
$\theta_{h\alpha}$ complex amplitude ratio
θ_{Lh} complex-valued ratio of the first harmonic of the lift to that of the plunging motion, N/rad
$\theta_{M\alpha}$ complex-valued ratio of the first harmonic of the moment to that of the pitching motion, Nm/rad

I. Introduction

Aeroelastic limit-cycle oscillations (LCOs) are caused by non-linearities in either the flow around an object or by non-linearities in the structure of the object, or a combination of both. In contrast to unbounded flutter, which can be predicted using a linearised analysis, the amplitude of an LCO remains constant. Hence, these limit-cycle oscillations cannot be predicted by a linearised method. This means that a linearised method might fail to predict flutter onset correctly if limit-cycle oscillations would already occur below flutter onset. Therefore, it is necessary to know if LCOs can indeed exist below the linear flutter point and at which flow conditions they exist or which structural properties are required for LCOs to exist.

Structural non-linearities are relatively easy to analyse. However, to investigate the aerodynamic sources of non-linearities extensive wind-tunnel tests or numerical codes capable of representing these non-linearities

are required. Nowadays, fluid-structure interaction coupling with the aerodynamic flow represented by a Computational Fluid Dynamics (CFD) code are used to analyse limit-cycle oscillations. However, these simulations are computationally expensive and cannot be used for extensive parameter studies. Furthermore, unstable LCOs as well as multiple nested LCOs cannot be found directly from coupled fluid-structure interaction simulations. Therefore, the well-known p-k method, used in classical (linear) flutter analysis, has been extended for the prediction of limit-cycle oscillations, see van Rooij et al.[1–3] This method allows one to extensively study the Hopf bifurcation behaviour of limit-cycle oscillation solutions, due to the reduced computational time once the aerodynamic response is known as a function of the frequencies, amplitudes and phase differences of the degrees of freedom. Figure 1 shows a sketch of the LCO amplitude as a function of the airspeed (after Dowell et al.[4]). Two types of bifurcations of the LCO amplitude can be distinguished; supercritical and subcritical bifurcations, also called benign and detrimental LCOs, respectively. In case of a supercritical bifurcation, LCOs only exist at airspeeds larger than the (linearised) flutter speed. Depending on the strength of the non-linearity, the slope of the bifurcation diagram is either large (when the non-linearity is weak) or small (when the non-linearity is strong). In case of a subcritical bifurcation, LCOs would already exist at speeds below the (linearised) flutter speed U_{∞_f}. Hence, they are referred to as detrimental. The arrows in Figure 1 indicate that for the subcritical bifurcation, the lower branch (dashed red line) consists of unstable LCOs, whereas the upper branch consists of stable LCOs.

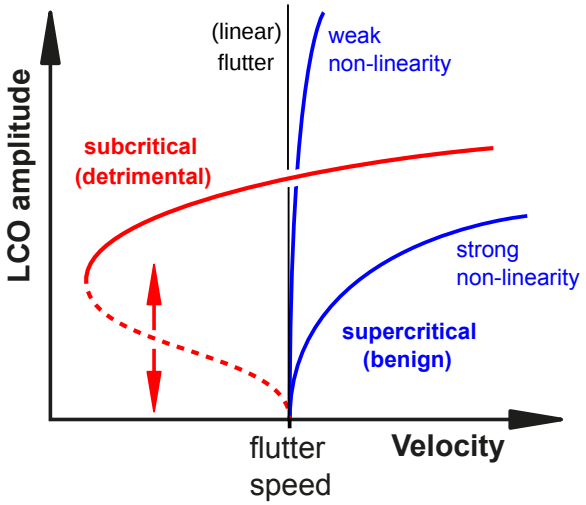

Figure 1. Sketch of LCO bifurcation behaviour (after Dowell et al.[4])

Studies of the bifurcation behaviour of LCO solutions caused by aerodynamic non-linearities are rare[5–12] and to the author's knowledge, only two of these studies have found subcritical bifurcations. Kholodar et al.[6,7] have found subcritical bifurcations of the NACA64A010A airfoil in inviscid flow using the harmonic balance (HB) method, whereas Balajewicz and Dowell[12] observed subcritical bifurcation behaviour for the NACA0012 airfoil in inviscid flow (also using the HB method). Furthermore, Kholodar et al.[6,7] are, to the author's knowledge, the only researchers that systematically studied the effect of Mach number and structural parameter variations. They observed that there is a high sensitivity of the LCO behaviour with respect to Mach number and uncoupled natural structural frequency ratio, especially in the transonic regime. The mass ratio had a less significant impact on the LCO bifurcation behaviour. However, Kholodar et al.[6,7] did not analyse the LCO bifurcation behaviour and its corresponding source (the aerodynamic forces) in detail. Why does a certain bifurcation behaviour establish itself? And can this behaviour be correlated with the behaviour of the flow and/or the structure? Furthermore, the two previous studies mentioned here only considered inviscid flow, but what happens in viscous flow, when the aerodynamic non-linearity is expected to be much stronger due the presence of and/or the interaction with the boundary layer? Can subcritical bifurcations of the LCO amplitude also exist in viscous transonic flow?

Hence, this paper studies the LCO bifurcation behaviour of a two degree-of-freedom (DoF) airfoil in both inviscid and viscous transonic flow. It will be investigated whether limit-cycle oscillations can already occur below the flutter boundary predicted from linearised theory, i.e. whether subcritical bifurcations of the LCO amplitude can exist, by varying several properties of the (linear) structural model, as well as the Mach number in inviscid flow. Especially in viscous flow where the non-linearity is expected to be larger than in inviscid flow due to the interaction of the shock-waves and the boundary layer. Furthermore, the relation between the aerodynamic forces and the bifurcation behaviour is studied in order to establish the local and global sources of the amplitude limitation.

This paper will first shortly address the computational method used, i.e. the amplitude-dependent p-k method and the CFD simulations necessary. Then the results of three separates studies will be shown in Section III. First, the effects of variations of two parameters of the structural model on the bifurcation behaviour in both viscous and inviscid transonic flow will be shown. Then, the Mach number is varied in inviscid flow. The effect of this variation on the flutter and LCO behaviour is shown in Section B. Finally, the response surface is analysed and compared to the bifurcation behaviour in Section C and conclusions are drawn in Section IV.

II. Computational Method

To study limit-cycle oscillations of a two degree-of-freedom airfoil system, the amplitude-dependent p-k method (ADePK) as presented by van Rooij et al.[2,3] is used. A short overview of this method is given here, more details can be found in van Rooij et al.[2,3] Figure 2 shows the two-degree-of-freedom airfoil system without structural damping.

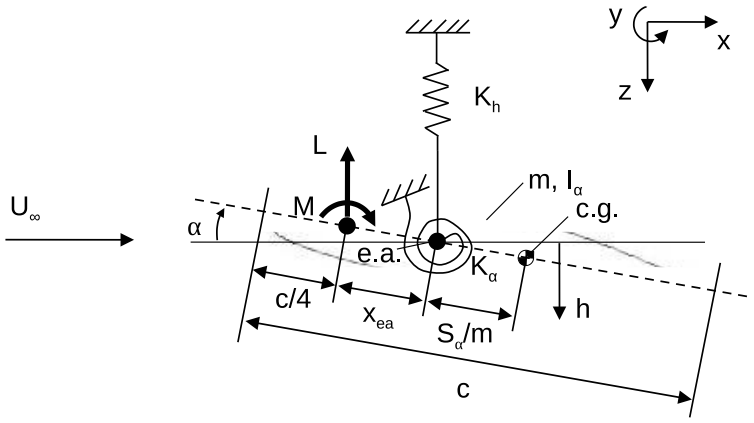

Figure 2. Sketch of the model with two degrees of freedom

The equations of motion of this system are given by:

$$\underbrace{\begin{bmatrix} m & S_\alpha \\ S_\alpha & I_\alpha \end{bmatrix}}_{\mathbf{M}} \underbrace{\begin{bmatrix} \ddot{h} \\ \ddot{\alpha} \end{bmatrix}}_{\ddot{\vec{x}}} + \underbrace{\begin{bmatrix} K_h & 0 \\ 0 & K_\alpha \end{bmatrix}}_{\mathbf{K}} \underbrace{\begin{bmatrix} h \\ \alpha \end{bmatrix}}_{\vec{x}} = \underbrace{\begin{bmatrix} -L \\ M + x_{\mathrm{ea}} \cdot L \end{bmatrix}}_{\vec{f}}. \tag{1}$$

Here m is the mass, I_α the mass moment of inertia, S_α the static moment, K_α the torsional stiffness, L the aerodynamic lift, M the moment about the quarter-chord point, and $M + x_{\mathrm{ea}} \cdot L$ the aerodynamic moment about the elastic axis, where x_{ea} is the distance between the quarter-chord point and the elastic axis (positive aft). The plunge displacement and the pitch angle are represented by h and α, respectively.

In the amplitude-dependent p-k method, the equations of motion are transformed into the frequency domain by assuming a first-harmonic sinusoidal solution (as in the conventional p-k method developed by Hassig[13]). Hence, a solution of the form $\vec{x} = \hat{\vec{x}} e^{pt}$, with $p = \delta + i\omega$ the eigenvalue, and $\hat{\vec{x}}$ the complex-valued motion vector, is assumed. The symbols δ and ω denote the amplification rate and the angular frequency,

respectively. Inserting this assumed solution into the equations of motion (1), leads to:

$$p^2\mathbf{M}\vec{\hat{x}} + \mathbf{K}\vec{\hat{x}} = \vec{\hat{f}}\left(k, \vec{\hat{x}}\right), \tag{2}$$

where k denotes the reduced frequency given by: $k = \omega c/U_\infty$. The complex-valued motion vector is defined as:

$$\vec{\hat{x}} = \begin{bmatrix} \theta_{h\alpha} \cdot c \\ 1 \end{bmatrix} \cdot \Delta\alpha,$$

where $\theta_{h\alpha}$ is the complex-valued amplitude ratio, c the chord length of the airfoil and $\Delta\alpha$ the pitch amplitude. The magnitude and phase angle of the complex-valued amplitude ratio $\theta_{h\alpha}$ are given by $|\theta_{h\alpha}|$ and $\phi_{h\alpha}$, respectively.

The aerodynamic forces are represented by a first harmonic sinusoidal motion as well: $\vec{f} = \vec{\hat{f}}e^{pt}$, where, as in the conventional p-k method, $\vec{\hat{f}}$ is only a function of k and not of p. However, in contrast to the linearised case, the aerodynamic forces cannot be represented by a generalised aerodynamic force (GAF) matrix $\mathbf{A}(k)$ times $\vec{\hat{x}}$ (i.e. $\vec{\hat{f}} \neq \mathbf{A}\vec{\hat{x}}$), due to the non-linear dependency of the aerodynamic forces on all mode shape parameters (ω, $\Delta\alpha$, and the complex-valued amplitude ratio $\theta_{h\alpha}$). Therefore, the relations between the aerodynamic forces (complex aerodynamic lift and moment) and the mode shape parameters need to be established in the form of a so-called response surface, which is constructed a-priori using harmonic forced motion CFD simulations. The aerodynamic forces are then computed by interpolation on this response surface during the iterations of the amplitude-dependent p-k method solver. Since there are more unknowns (3, i.e. p, $\Delta\alpha$, and $\theta_{h\alpha}$) than equations (2, i.e. (1)), the equations of motion are solved at a pre-set pitch amplitude $\Delta\alpha$. By solving the equations of motion for various pre-set amplitudes, the amplitude at which the amplification rate δ equals zero can be found. This is the LCO amplitude. Furthermore, the stability of the LCO can be determined from the slope of the δ-$\Delta\alpha$-diagram. Hence, from ADePK both stable and unstable LCOs can be found. The other LCO mode shape parameters follow from (2). Further details on the amplitude-dependent p-k method can be found in van Rooij et al.[2,3]

The response surfaces for the complex-valued aerodynamic lift and moment are generated using CFD simulations with a finite-volume, cell-vertex-based, unstructured, compressible solver for both the Reynolds-Averaged Navier-Stokes (RANS) and the Euler equations. The DLR-TAU CFD-code[14] has been used in this work. Both viscous and inviscid CFD computations have been performed. For spatial discretisation a 2nd-order central scheme[15] is used. Temporal discretisation is realised by dual time stepping,[16] where in order to integrate in physical time, the implicit 2nd-order accurate Backward Differencing Formula (BDF2) integration scheme has been used. At each physical time step, the governing equations are integrated explicitly by adding a so-called pseudo time derivative. The Menter SST turbulence model[17] has been used for the RANS simulations.

The unstructured mesh used for the inviscid CFD simulations has 10369 points. This mesh was investigated to be sufficiently fine to give mesh independent results. For the viscous flow computations a structured mesh with 65888 points was used. The non-dimensional first cell height of this mesh was estimated to be 0.75. This mesh was also found to give mesh independent results.[1]

The supercritical NLR7301 airfoil is used to study LCO behaviour in this work, since it has already been subject of numerous experimental[18–22] and numerical investigations[5,23–32] regarding limit-cycle oscillations. Table 1 shows the flow conditions at which the viscous and inviscid simulations have been performed. Note that the Mach number has been varied for the inviscid flow simulations.

Parameter	Euler	RANS
M_∞	0.55-0.8	0.75
$\bar{\alpha}$	0°	0.7°
Re	-	$2 \cdot 10^6$
T_∞	273.15 K	273.15 K
p_∞	101325 Pa	-

Table 1. Flow conditions for the CFD simulations

The structural properties of the wind-tunnel model of Dietz et al.[21] are used for the investigations in this work (with zero structural damping). These structural parameters were used as the nominal structural parameters, see Table 2. In Section 1, K_h and x_{ea} will be varied independently. Note that the nominal location of the elastic axis is at the quarter-chord point.

Structural parameter	Value	Units
Wing span b	1.0	m
Chord length c	0.3	m
Mass m	26.268	kg
Mass moment of inertia (about the elastic axis) I_α	0.079	kgm^2
Torsional spring stiffness K_α	$6.646 \cdot 10^3$	Nm/rad
Plunge spring stiffness K_h	$1.078 \cdot 10^6$	N/m
Static moment (related to EA) S_α	0.331	kgm
Distance between quarter-chord point and elastic axis x_{ea}	0	m

Table 2. Structural parameters for the two DoF NLR7301 airfoil system (taken from Dietz et al.[21])

The response surface of the aerodynamic forces has been generated using a tensor-product grid of sample points in this work. The aerodynamic forces at each sample point have been computed from a harmonic forced motion simulation of the airfoil at a particular frequency, pitch amplitude and complex amplitude ratio. The response surface sample locations are shown in Table 3 for the viscous test case of this work. For the inviscid test case the same samples have been used except for the samples at $\Delta\alpha = 4°$. At zero pitch amplitude the aerodynamic forces are identically zero and at $k = 0$, the aerodynamic forces have been determined from the difference of two steady simulations at each amplitude. This results in a total of 1280 sample points for the viscous flow test case and 1120 sample points for the inviscid flow test cases. Is is noted here that the response surface is set up at a certain reference velocity and hence the results obtained with ADePK are non-matched, see van Rooij et al.[3] Interpolation of the response surface is applied using cubic spline interpolation.

Parameter	Values
Pitch amplitude $\Delta\alpha(°)$	0, 0.1, 0.5, 1, 2, 3, 4, 5
Amplitude ratio $\lvert\theta_{h\alpha}\rvert$	0.01, 0.75, 2, 4
Reduced frequency k	0, 0.1, 0.2, 0.3, 0.4, 0.5, 0.6, 0.7
Phase difference $\phi_{h\alpha}(°)$	5, 10, 50, 100, 150

Table 3. CFD sample locations

III. Results

This section shows the bifurcation behaviour of the limit-cycle oscillation solutions obtained with the ADePK method. The NLR7301 airfoil is studied in two types of flow; a viscous transonic flow at $M = 0.75$ and $\bar{\alpha} = 0.7°$, and an inviscid flow at $M = 0.74$, $\bar{\alpha} = 0°$. The steady pressure coefficient and skin friction coefficient distributions are shown in Figure 3. The continuous line displays the upper surface and the dashed line the lower surface. A black horizontal line has been drawn at the critical pressure. For the inviscid case a strong shock wave is present on the upper surface near 65% of the chord length, see Figure 3(a). For the viscous a shock wave is present on the upper surface near the mid-chord position (see Figure 3(b)) and trailing-edge separation occurs on this surface as well (see Figure 3(c)).

The results of the effect of several structural parameters changes on the bifurcation behaviour of the LCO solutions from the two test cases shown in Figure 3 are studied in Section A. Then the Mach number is varied in inviscid flow. The flutter boundary as well as the LCO bifurcation behaviour is computed for each Mach number, see Section B. Finally, the response surface used to compute the aerodynamic forces during

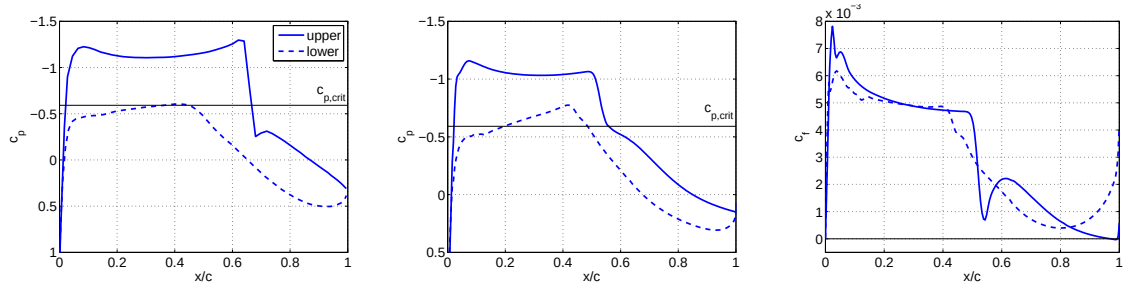

(a) c_p vs. x/c in inviscid flow at $M = 0.74$, $\bar{\alpha} = 0°$

(b) c_p vs. x/c in viscous flow at $M = 0.75$, $\bar{\alpha} = 0.7°$

(c) c_f vs. x/c in viscous flow at $M = 0.75$, $\bar{\alpha} = 0.7°$

Figure 3. Steady pressure and skin friction distributions

the iterations of ADePK and its relation to the LCO bifurcation behaviour is studied in Section C.

A. Structural parameter variations

Two structural parameters have been varied; the structural uncoupled natural frequency ratio ω_h/ω_α, and the elastic axis location x_{ea}. This section shows the bifurcation behaviour of the LCO solutions in terms of the LCO amplitude, the LCO mode shape, and the LCO reduced frequency as a function of the freestream velocity in inviscid and viscous flow.

1. Structural frequency ratio

The structural uncoupled natural frequency ratio, or structural frequency ratio (SFR) for short, has been varied from 0.49 to 1.21. In order to achieve this, the plunge stiffness K_h has been changed. The remaining structural parameters are constant (see Table 2). Figure 4 shows the LCO amplitudes versus the freestream speed normalised by the flutter speed for the NLR7301 airfoil in inviscid flow at $M_\infty = 0.74$ and $\bar{\alpha} = 0°$. Figure 5 shows the bifurcation diagrams of the LCO mode shape parameters and the LCO reduced frequency versus the freestream speed U_∞. Figure 5(e) shows the phase difference versus the amplitude ratio. From Figure 4 it is immediately clear that for small values of ω_h/ω_α the bifurcation is subcritical. For larger SFRs, the bifurcation is supercritical. For these large SFRs, the slope of the bifurcation diagram decreases with increasing SFR. This indicates that the non-linearity becomes larger when the SFR is increased from 0.74 to 1.21 (see Figure 1). From Figure 5(b), the amplitude ratio $|\theta_{h\alpha}|$ decreases with increasing SFR. During the bifurcation, the amplitude ratio decreases with freestream speed for SFRs from 0.83 till 1.04. For larger SFRs, $|\theta_{h\alpha}|$ increases with increasing U_∞, whereas for smaller SFRs, the amplitude ratio shows a more complicated bifurcation behaviour. The phase difference $\phi_{h\alpha}$ first decreases somewhat, but then increases up to about 110° at $\omega_h/\omega_\alpha = 1.21$. For $\omega_h/\omega_\alpha \geq 0.74$, $\phi_{h\alpha}$ increases during the bifurcation. For smaller SFRs, the bifurcation behaviour of $\phi_{h\alpha}$ is more complicated. The reduced frequency at flutter increases up to an SFR of 0.90, then it decreases with increasing SFR. This is caused by the inverse relation of the reduced frequency with the freestream velocity ($k = \omega c/U_\infty$). This relation also dictates the bifurcation behaviour of the reduced frequency (as a function of the freestream velocity).

As expected because of the structural frequency ratio values, Figure 5(e) shows a plunge-dominated mode shape for small SFRs with a large amplitude ratio and a pitch-dominated mode shape for large SFR (with an amplitude ratio $\ll 1$). For the inviscid flow test case considered here, at small SFRs a subcritical bifurcation occurs that has a plunge-dominated mode shape, whereas the pitch-dominated cases are supercritical. In contrast, Kholodar et al.[7] observed supercritical bifurcations which are plunge dominated at $\omega_h/\omega_\alpha = 0.5$ and subcritical bifurcations which are pitch dominated at $\omega_h/\omega_\alpha = 1.8$ for the NACA64010A airfoil in inviscid flow. To further investigate these differences in bifurcation behaviour, the structural frequency ratio of the NLR7301 airfoil was varied for two other Mach numbers in inviscid flow. From a SFR-variation of the NLR7301 airfoil at $M_\infty = 0.75$, $\bar{\alpha} = 0°$ in inviscid flow, unstable LCOs with a plunge- as well as a pitch-dominated mode shape were found as well. For $M_\infty = 0.72$ on the other hand, plunge dominated LCO solutions that undergo supercritical bifurcations were observed at small SFRs. These observations suggest

that there is no correlation between the type of bifurcation (i.e. supercritical or subcritical) that occurs and the mode shape (i.e. pitch- or plunge-dominated) in inviscid flow.

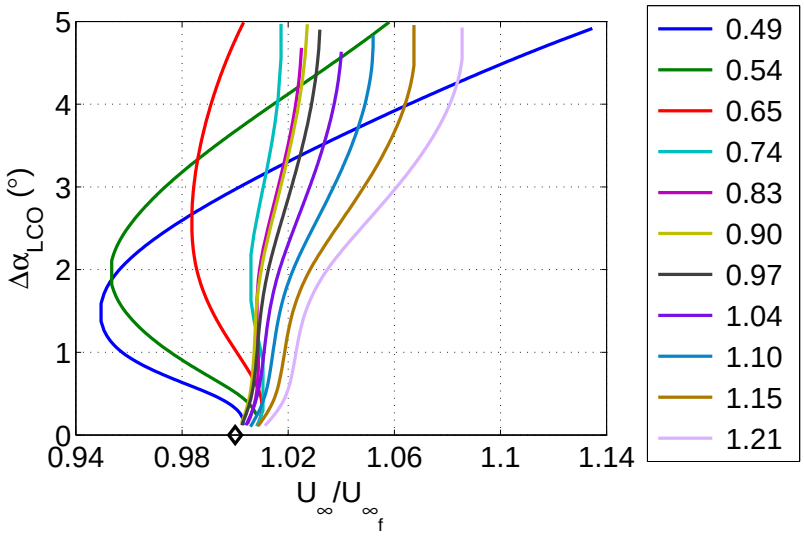

Figure 4. LCO pitch amplitude vs freestream velocity normalised by the linear flutter speed for a structural frequency ratio variation at $M_\infty = 0.74$, $\bar{\alpha} = 0°$ in inviscid flow

The results of an SFR-variation in case of transonic flow with trailing-edge separation ($M_\infty = 0.75$, $\bar{\alpha} = 0.7°$, $\mathrm{Re} = 2 \cdot 10^6$) are shown in Figures 6 and 7, which show the LCO mode shape and frequency versus the freestream velocity and the LCO amplitude versus the freestream velocity normalised by the flutter speed, respectively. For this test case it is observed that the bifurcation behaviour is supercritical for SFRs up to and including 1.21. Therefore, the bifurcation behaviour has been investigated at $\omega_h/\omega_\alpha = 1.56$ as well. At this SFR the bifurcation behaviour becomes subcritical. For SFRs smaller than 1.56, from Figure 7 the velocity range covered by the LCOs up to $\Delta\alpha_{LCO} = 5°$ initially increases with increasing SFR (i.e. the slope of the bifurcation diagram for amplitudes larger than about 1° decreases). Then at $\omega_h/\omega_\alpha = 0.83$ the velocity range is maximal (and the slope minimal), whereas for $\omega_h/\omega_\alpha > 0.83$, the velocity range decreases. Hence, for the supercritical bifurcations, the non-linearity becomes stronger with increasing SFR up to a value of 0.83, and for larger ω_h/ω_α the non-linearity diminishes again. For $\omega_h/\omega_\alpha = 1.56$ the non-linearity is again stronger.

For all SFRs, except for the largest four, the phase difference starts at a small value and increases with freestream speed. For $\omega_h/\omega_\alpha = 1.15$ and 1.21 the phase difference starts at 100° or above. At $\omega_h/\omega_\alpha = 1.56$ the phase difference increases with decreasing freestream speed. Note that at this SFR the phase difference has been extrapolated, since the largest sample point is at $\phi_{h\alpha} = 150°$. Figure 6(e) clearly shows the large range of phase difference covered by SFRs near 1. Furthermore, at small SFR the LCOs are stable, the mode shape is plunge-dominated and $|\theta_{h\alpha}|$ decreases with increasing U_∞. At large SFR the LCOs are stable at small to moderate amplitudes and unstable at large amplitudes, the mode shape is pitch-dominated and $|\theta_{h\alpha}|$ first increases with increasing U_∞ and then increases further with decreasing U_∞. This behaviour is similar to that observed by Kholodar et al.[7] However, it is in contrast to that of the inviscid flow test case of Figures 4 and 5. The reduced frequency at flutter shows similar behaviour as the inviscid flow test case, i.e. it increases with increasing SFR up until 0.90, for larger SFRs it decreases. Furthermore, as expected due to the inverse relation with U_∞, for the supercritical bifurcations the reduced frequency decreases with freestream speed, whereas at the largest two SFRs k first decreases and then increases.

From the results of these two test cases it can be concluded that variation of the structural uncoupled natural frequency ratio significantly influences the LCO bifurcation behaviour. Especially when the non-linearity is relatively weak as for the inviscid case shown in this section, the bifurcation type can change. For the viscous test case, the bifurcation type did not change under a variation of the structural frequency ratio from 0.49 to 1.21. However, it is changes when the structural frequency ratio is increased further to 1.56.

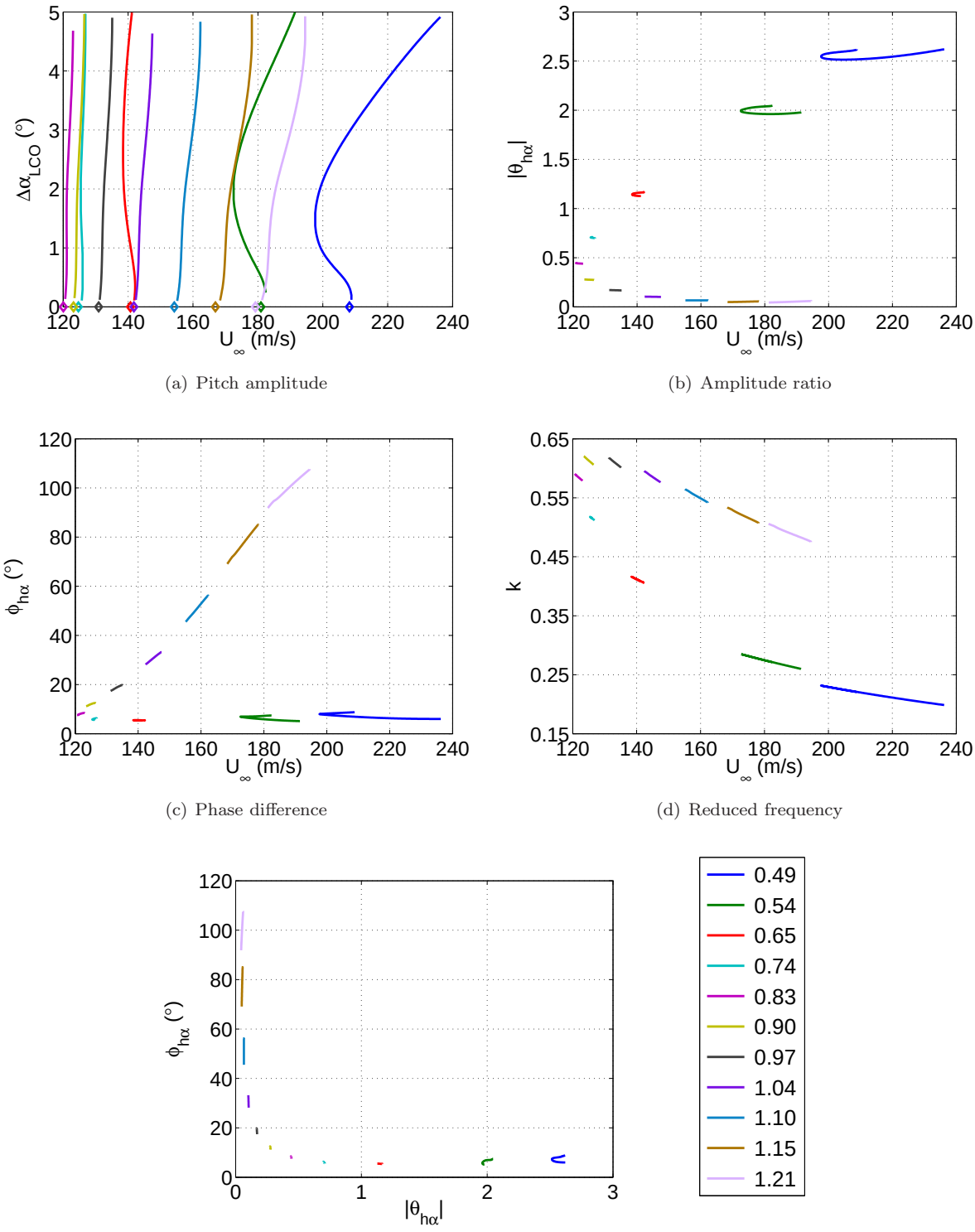

(a) Pitch amplitude

(b) Amplitude ratio

(c) Phase difference

(d) Reduced frequency

(e) Phase difference vs. amplitude ratio

(f)

Figure 5. LCO mode shape vs freestream velocity for a structural frequency ratio variation at $M_\infty = 0.74$, $\bar{\alpha} = 0^\circ$ in inviscid flow

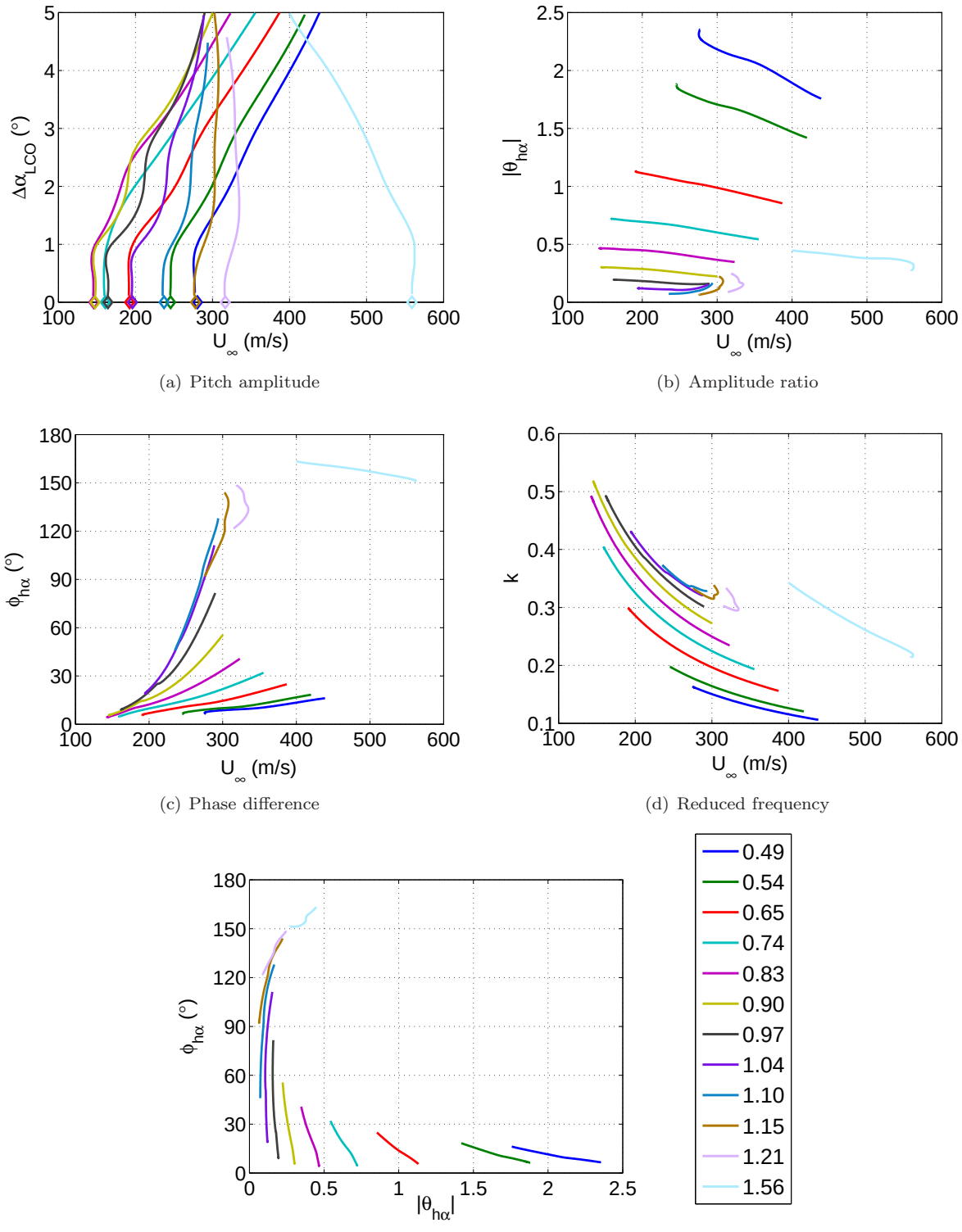

(a) Pitch amplitude

(b) Amplitude ratio

(c) Phase difference

(d) Reduced frequency

(e) Phase difference vs. amplitude ratio

(f)

Figure 6. LCO mode shape vs freestream velocity for a structural frequency ratio variation at $M_\infty = 0.75$, $\bar{\alpha} = 0.7°$ in viscous flow

2. Elastic axis location

In order to investigate the generality of the results obtained in this work, the elastic axis location has been varied, keeping the remaining parameters constant (the static moment S_α and the mass moment of inertia

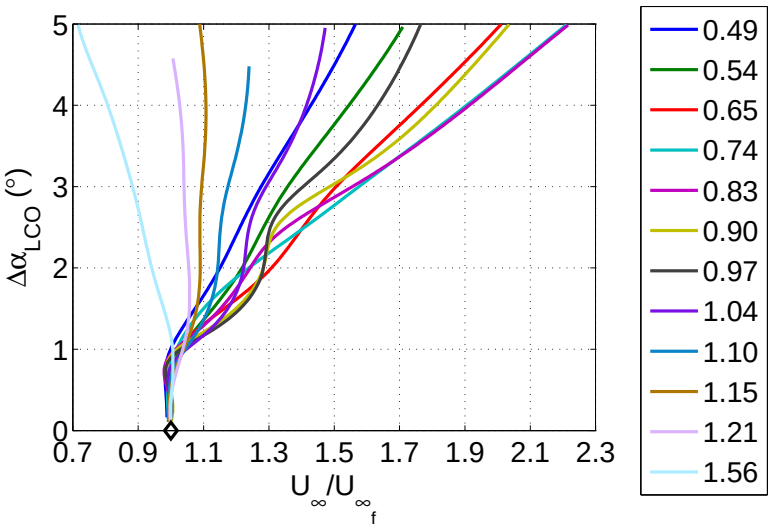

Figure 7. LCO pitch amplitude vs freestream velocity normalised by the linear flutter speed for a structural frequency ratio variation at $M_\infty = 0.75$, $\bar{\alpha} = 0.7°$ in viscous flow

I_α as well). Figures 8 and 9 show the result in terms of the bifurcation behaviour for the inviscid test case at $M_\infty = 0.74$, $\bar{\alpha} = 0°$ and for viscous test case at $M_\infty = 0.75$, $\bar{\alpha} = 0.7°$, respectively. Note that the non-dimensional elastic axis location from the quarter-chord point is shown in the legend of these figures, where a positive distance indicates that the elastic axis is located aft of the quarter-chord point, see Figure 2. Figure 8 shows a change in bifurcation behaviour from subcritical to supercritical with increasing aft location of the elastic axis for the test case in inviscid transonic flow. From Figure 9 it is observed that, for the viscous flow test case, the slope of the supercritical bifurcation increases when the elastic axis is located further aft of the quarter-chord point, i.e. the non-linearity becomes weaker. However, the bifurcation type remains the same. For this test case, the amplitude ratio decreases with increasing freestream velocity, except when the elastic axis is located upstream of the quarter-chord point, then it first increases and then decreases, see Figure 9(b). For the inviscid test case the amplitude ratio decreases during the bifurcation for all x_{ea}, see Figure 8(b). At $M_\infty = 0.74$, $\bar{\alpha} = 0°$ the phase difference shows a complicated bifurcation behaviour, see Figure 8(c), whereas the phase difference increases with increasing freestream velocity for all elastic axis locations at $M_\infty = 0.75$, $\bar{\alpha} = 0.7°$. When the elastic axis is located at 75% of the chord length, i.e. 0.5c behind the quarter-chord point, the phase difference increases dramatically for the viscous flow test case. This happens at very small amplitude ratios, as can been from Figure 9(e). This means that for $x_{\text{ea}} = 0.5c$, the LCO mode shape becomes almost a pure pitch motion where plunge leads pitch. For both test cases, the reduced frequency increases with increasing distance between the quarter-chord point and the elastic axis, although it decreases with increasing freestream velocity for a particular elastic axis position, as expected due to the inverse relation with the freestream velocity.

Increasing the structural frequency ratio to 1.21 for the viscous test case results in a change of bifurcation type as illustrated in Figure 10. Note that the most aft elastic axis location is no further than 35% of the chord length aft of the quarter-chord point, because no flutter was observed for more aft locations of the elastic axis. For the transonic inviscid test case, a transition from subcritical to supercritical bifurcation behaviour at the nominal structural frequency ratio (0.70) is observed when the elastic axis is moved aft. Hence, these results show that, when the elastic axis location is shifted, the strength of the non-linearity changes and a change in bifurcation behaviour may occur.

B. Mach number variation in inviscid flow

Figure 11(a) shows the flutter speed U_{∞_f} versus the Mach number at a mean angle of attack of 0° (as obtained from the conventional p-k method). The nominal structural parameters as shown in Table 2 have been used in this section. The flutter speed decreases with increasing Mach number, at transonic Mach numbers a minimum is reached, the so-called "transonic dip". The flutter boundary shown in Figure 11(a)

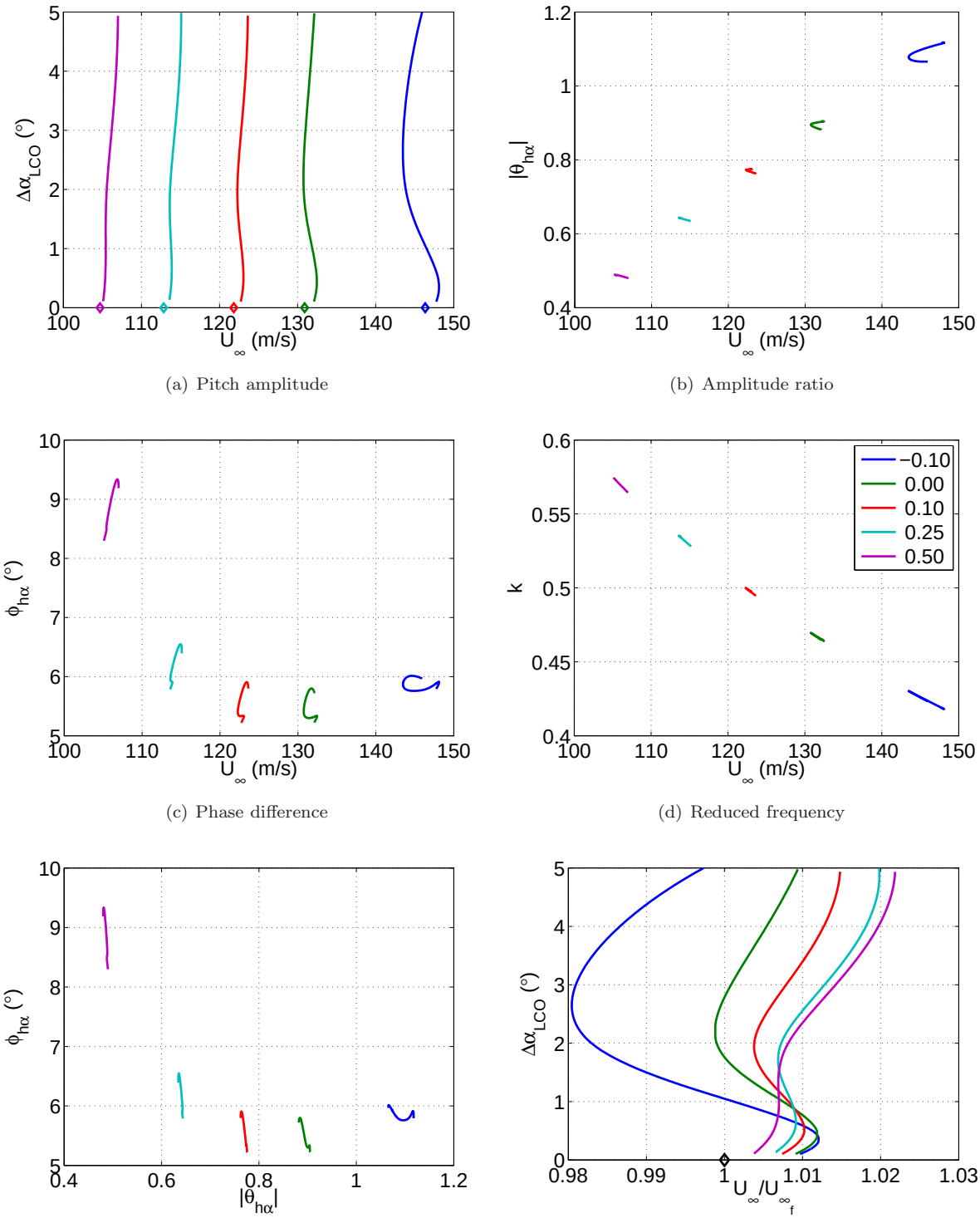

(a) Pitch amplitude

(b) Amplitude ratio

(c) Phase difference

(d) Reduced frequency

(e) Phase difference vs. amplitude ratio

(f) Pitch amplitude

Figure 8. LCO mode shape vs freestream velocity for a variation of the non-dimensional elastic axis location at $M_\infty = 0.74$, $\bar{\alpha} = 0°$ in inviscid flow (value of x_{ea}/c is shown in the legend)

shows two transonic dips, at $M_\infty = 0.72$ and at $M_\infty = 0.78$. The plunge mode was the first mode to become unstable for all Mach numbers. At Mach numbers of 0.76 and larger the second mode, the pitch mode,

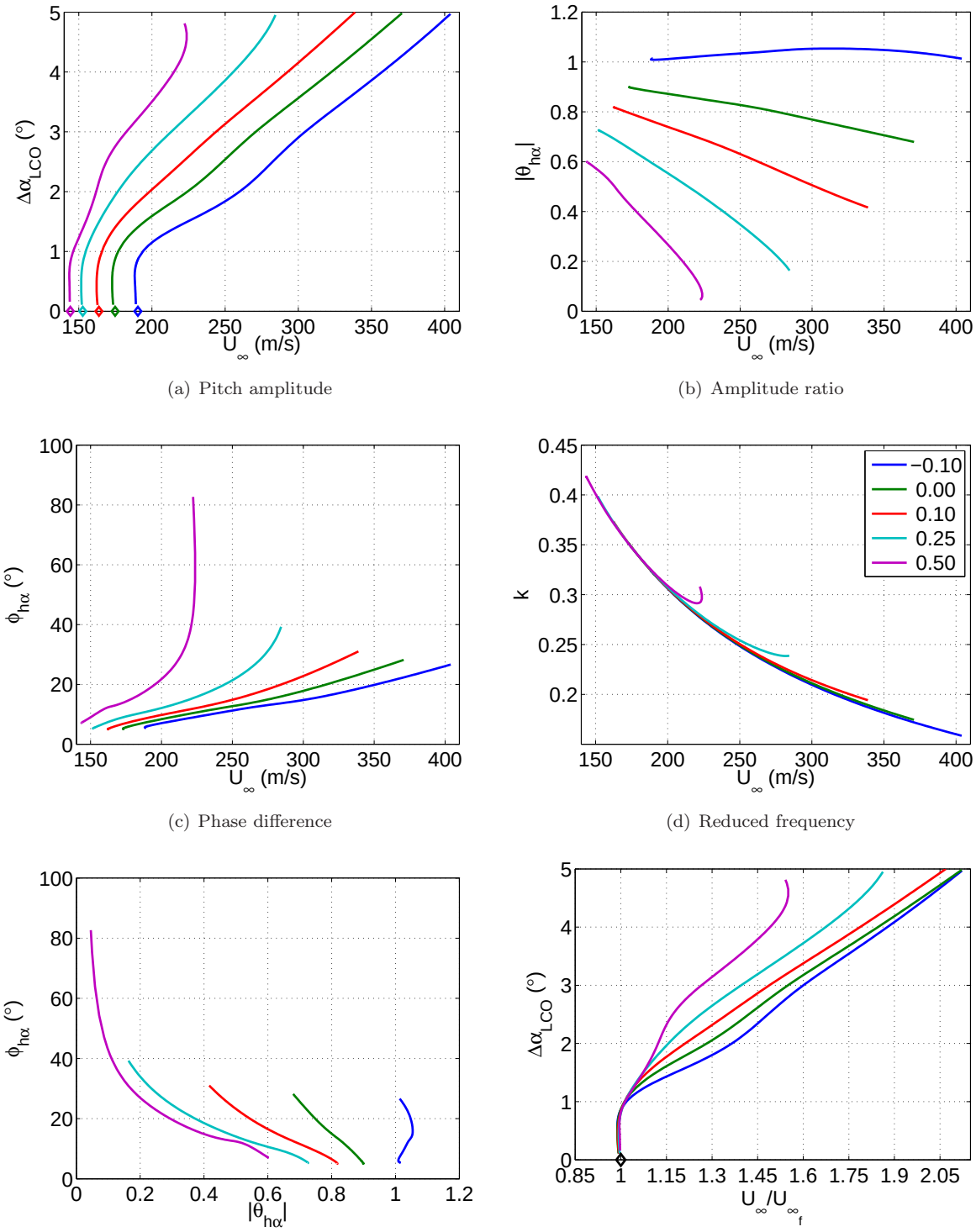

(a) Pitch amplitude

(b) Amplitude ratio

(c) Phase difference

(d) Reduced frequency

(e) Phase difference vs. amplitude ratio

(f) Pitch amplitude

Figure 9. LCO mode shape vs freestream velocity for a variation of the non-dimensional elastic axis location at $M_\infty = 0.75$, $\bar{\alpha} = 0.7°$ in viscous flow (value of x_{ea}/c is shown in the legend)

becomes unstable as well. However, this occurs at much higher freestream velocity then the plunge mode. Such a flutter boundary is typical for Euler-based flow calculations.[33] A similar-shaped flutter boundary

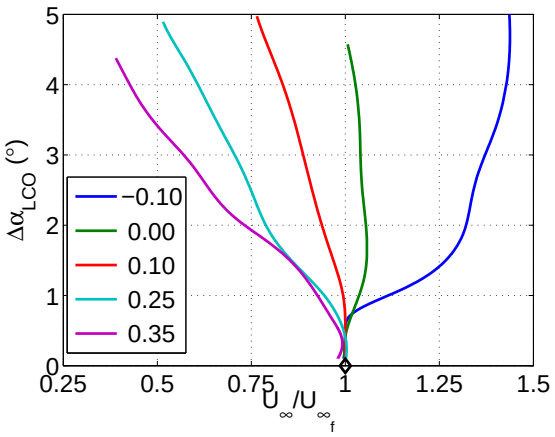

Figure 10. LCO mode shape vs freestream velocity normalised by the linear flutter speed for a variation of the non-dimensional elastic axis location at $M_\infty = 0.75$, $\bar{\alpha} = 0.7°$, $\omega_h/\omega_\alpha = 1.21$ in viscous flow (value of x_{ea}/c is shown in the legend)

was found by Yang et al.[33] and Hall et al.[34] for the NACA64A010 airfoil. The secondary unstable mode disappears in viscous flow. Therefore, in this work only the first unstable mode will be considered in the study of the LCO behaviour of the NLR7301 airfoil.

Figure 11 also shows the reduced frequency k_f, amplitude ratio $|\theta_{h\alpha}|_f$ and phase difference $(\phi_{h\alpha})_f$ at flutter versus the Mach number at a mean angle of attack of 0°. As expected, the reduced frequency at flutter increases with increasing Mach number and shows the opposite behaviour of the freestream speed, since a maximum is obtained at $M_\infty = 0.72$ and $M_\infty = 0.78$. The amplitude ratio at flutter increases from 0.72 at $M_\infty = 0.55$ to about 0.9 at transonic Mach numbers. Similar behaviour was observed by Kholodar et al.[6,7] for the amplitude ratio at flutter at an ω_h/ω_α of 0.8 for the NACA64A010A airfoil. (Here $\omega_h/\omega_\alpha = 0.70$.) The phase difference between pitch and plunge at flutter increases from about 9° at $M_\infty = 0.55$ to about 15° at $M_\infty = 0.71$ and then decreases until to almost 0° at $M_\infty = 0.8$. Hence, the lag of the pitching motion w.r.t. the plunging motion first increases, and then decreases again.

The ADePK method has been used to compute the bifurcation behaviour at several Mach numbers ($M_\infty = 0.55$, 0.6, 0.65, 0.7, 0.72, 0.74, 0.75 and 0.8). Figure 12 shows contours levels of the LCO amplitude at several Mach numbers versus the freestream velocity. The flutter boundary has also been included (zero amplitude). Stable LCOs are shown with circles and unstable LCOs with squares. The dashed lines connect the unstable LCOs and the full lines the stable LCOs. It is observed that at subsonic Mach numbers the contour lines are much closer than near the transonic dip. This means that the bifurcation diagrams are much steeper at subsonic Mach numbers than near the transonic dip. Furthermore, when LCOs of a certain amplitude are allowed, for example with an amplitude of 3°, the transonic dip would be less deep than in case of flutter (zero amplitude). Hence, the non-linearity is much stronger at $M_\infty = 0.72$ and $M_\infty = 0.75$ than at $M_\infty = 0.55$, 0.6 and 0.65. This can be seen more clearly from the bifurcation diagrams shown in Figure 13. This figure shows the LCO mode shape versus the freestream velocity. The bifurcation of the LCO amplitude is supercritical for the smallest two Mach numbers ($M_\infty = 0.55$ and 0.6). Then it becomes subcritical with increasing Mach number, i.e. for $M_\infty = 0.65$ and $M_\infty = 0.7$. The bifurcation becomes supercritical again when further increasing Mach number. At $M_\infty = 0.74$ multiple stable and unstable LCOs exists. At $M_\infty = 0.75$ the bifurcation is subcritical as well, with stable LCOs of noticeable amplitude (up to 5°) that occur below the flutter boundary. This is also seen in Figure 12. At $M_\infty = 0.8$ the bifurcation is supercritical. Figure 13(b) shows that amplitude ratio $|\theta_{h\alpha}|$ decreases during the bifurcation for most Mach numbers, except for $M_\infty = 0.7$. Hence, the LCO mode shape becomes slightly more pitch-dominated during the bifurcation of the LCO solution. Only at $M_\infty = 0.7$ the motion tends to become a more complex pitch-plunge motion. This is also depicted in Figure 14, which shows the phase difference versus the amplitude ratio. From Figure 13(c), the phase difference increases with freestream speed for Mach numbers up to 0.6. At $M_\infty = 0.65$ it increases with decreasing freestream velocity, whereas for $M_\infty = 0.72$ it decreases with increasing U_∞. For $M_\infty = 0.7$ and the largest three Mach numbers the phase difference

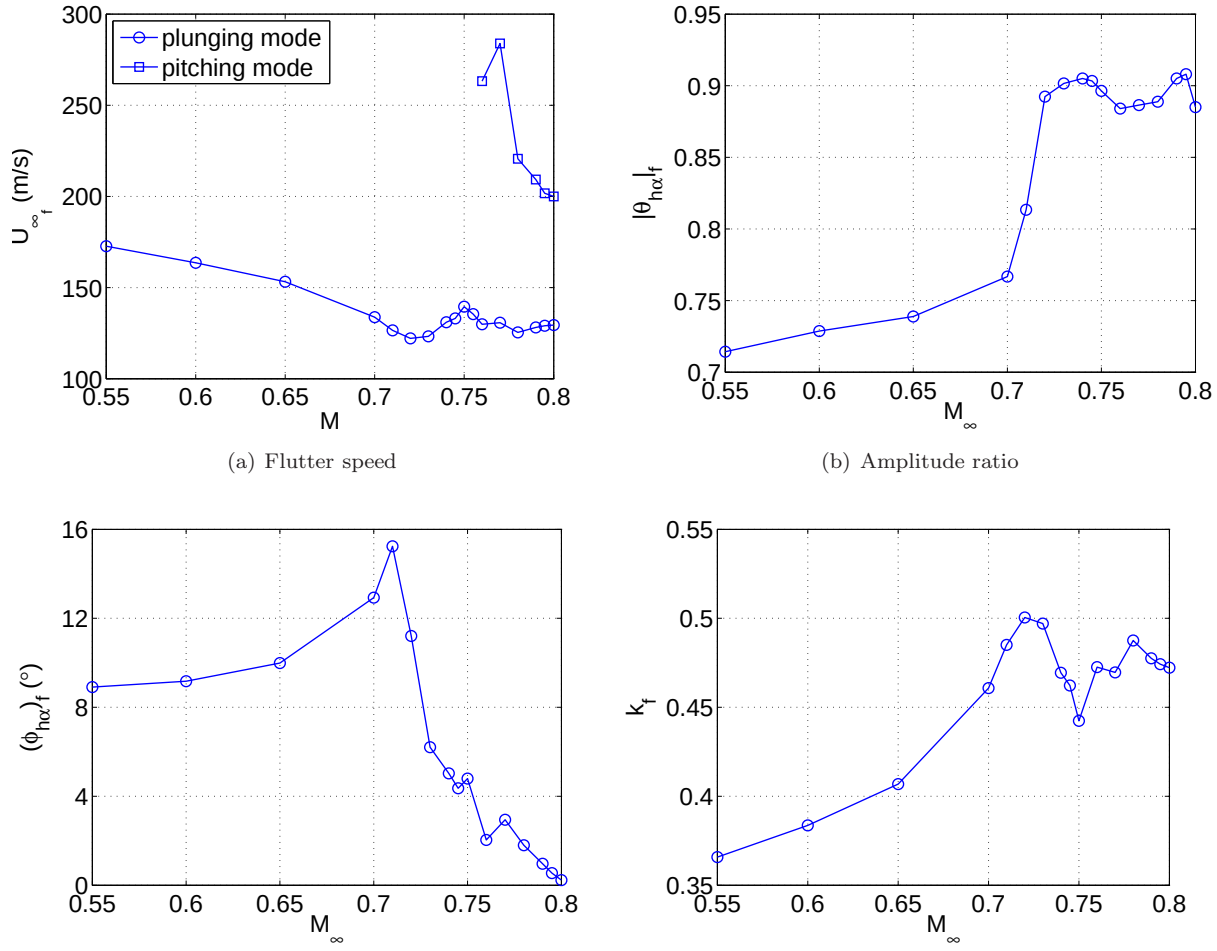

(a) Flutter speed

(b) Amplitude ratio

(c) Phase difference

(d) Reduced frequency

Figure 11. Flutter speed, reduced frequency, amplitude ratio and phase difference as a function of Mach number in inviscid flow

shows a more complex bifurcation behaviour. The same holds for the amplitude ratio at these Mach numbers. The bifurcation behaviour of the reduced frequency, shown in Figure 13(d), is again dictated by its inverse relationship with the freestream velocity.

Upon comparing the results obtained here with the Mach number variations performed by Kholodar et al.,[6,7] it is noted that they observed, at an ω_h/ω_α of 0.8, unstable LCOs (up to 7°) for Mach numbers far below the transonic dip (which is at about $M_\infty = 0.8$ in their case), whereas for the NLR7301 airfoil at $M_\infty = 0.55$ and $M_\infty = 0.6$ stable LCOs are observed. Closer to the transonic dip and in the transonic dip region itself, i.e. in the Mach number range from 0.78 to 0.85, Kholodar et al.[6,7] observed supercritical bifurcations for the NACA64A010A airfoil as also observed here (i.e. at $M_\infty = 0.72$). Directly after the dip the LCOs became unstable again and then stable again, as for the NLR7301 airfoil. Hence, except for the supercritical bifurcation behaviour for subsonic Mach numbers, the NLR7301 and the NACA64A010A airfoil seem to exhibit similar bifurcation behaviour close to the flutter boundary.

C. Response surface analysis

In order to investigate what non-linearity is responsible for the bifurcation behaviour, the magnitude and phase angle of the complex-valued ratios of the first harmonic of the lift to that of the plunging motion (i.e. $|\theta_{Lh}|$ and ϕ_{Lh}) and the magnitude and phase of the first harmonic of the moment to that of the pitching motion (i.e. $|\theta_{M\alpha}|$ and $\phi_{M\alpha}$), have been made constant (one-at-a-time analysis). The forces have each been

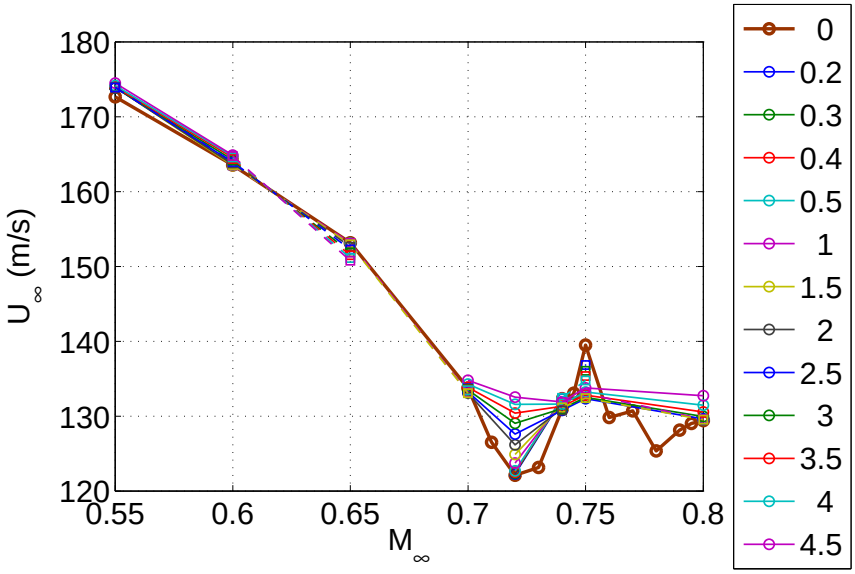

Figure 12. Flutter speed and LCO amplitude contours as a function of Mach number in inviscid flow

set, one at a time, to their value at $\Delta\alpha = 0.1°$. Then ADePK has been used to compute the bifurcation behaviour. The structural parameters are again those of the nominal structural model (see Table 2). This is performed for all Mach numbers of the inviscid Mach number test case shown in Section B as well as for the viscous test case at $M_\infty = 0.75$, $\bar{\alpha} = 0.7°$, $\mathrm{Re} = 2 \cdot 10^6$. Figure 15 shows the resulting bifurcation behaviour for the viscous test case as well as for inviscid flow at $M_\infty = 0.75$ and $\bar{\alpha} = 0°$.

From Figure 15 it is clearly seen that the setting the phase of the lift constant results in a completely different bifurcation behaviour for both test cases. The importance of the non-linearity in the phase of the lift (with increasing amplitude) was already observed by the authors in van Rooij et al.,[1] which discussed the energy budget of limit-cycle oscillations. At $M_\infty = 0.75$, $\bar{\alpha} = 0°$ the LCO amplitude increases rapidly in case of a constant phase of the lift. Holding the remaining parameters constant does have a small influence on the bifurcation behaviour, but this influence is not as significant as in case of ϕ_{Lh}. However, when keeping the magnitude of the moment $|\theta_{M\alpha}|$ constant at $M_\infty = 0.8$ (not shown here) in inviscid flow, the bifurcation behaviour is also somewhat different from the non-linear case for amplitudes up to 4°. Although the trend towards a supercritical bifurcation is the same as in the non-linear case. This cannot be concluded in case of a constant ϕ_{Lh} for this test case. For other Mach numbers in inviscid similar trends regarding the bifurcation behaviour when ϕ_{Lh} is held constant are observed. The results of the one-at-a-time constant aerodynamic force or moment analysis for the viscous flow test case at $M_\infty = 0.75$ and $\bar{\alpha} = 0.7°$ are shown in Figure 15(b). For this test case keeping ϕ_{Lh} constant also results in the most significant deviation from the actual (non-linear) bifurcation behaviour. Hence, from this study it can be concluded that the non-linearities in the phase of the lift are responsible for the type of bifurcation that occurs. In addition, for some test cases (e.g. $M_\infty = 0.8$, $\bar{\alpha} = 0°$ in inviscid flow) non-linearities in the magnitude of the moment might influence the bifurcation type.

Now the question is can the observations and conclusions from Figure 15 (and from the other Mach numbers in inviscid flow, which are not shown here) be used to link a certain bifurcation behaviour to the response surface? In other words given a certain response surface, which types of bifurcations can occur provided the right structural properties are available? To answer these questions the aerodynamic response surface has been analysed through various slices. During this analysis it was noted that at those amplitudes at which the stability of the LCO changes, i.e. at a saddle-node bifurcation of limit cycles,[35] the aerodynamic response surface also shows curvature changes. That is, the phase of the lift w.r.t. plunge shows curvature changes. Figure 16 depicts a slice of the response surface versus the pitch amplitude at $M_\infty = 0.75$ and $\bar{\alpha} = 0°$ in inviscid flow. The time domain reference samples at $|\theta_{h\alpha}| = 0.75$, $\phi_{h\alpha} = 5°$ and $k = 0.5$ and the interpolated response surface at this mode shape and frequency are shown in this figure by the squares and the blue dashed lines, respectively. This mode shape is close to the flutter mode shape,

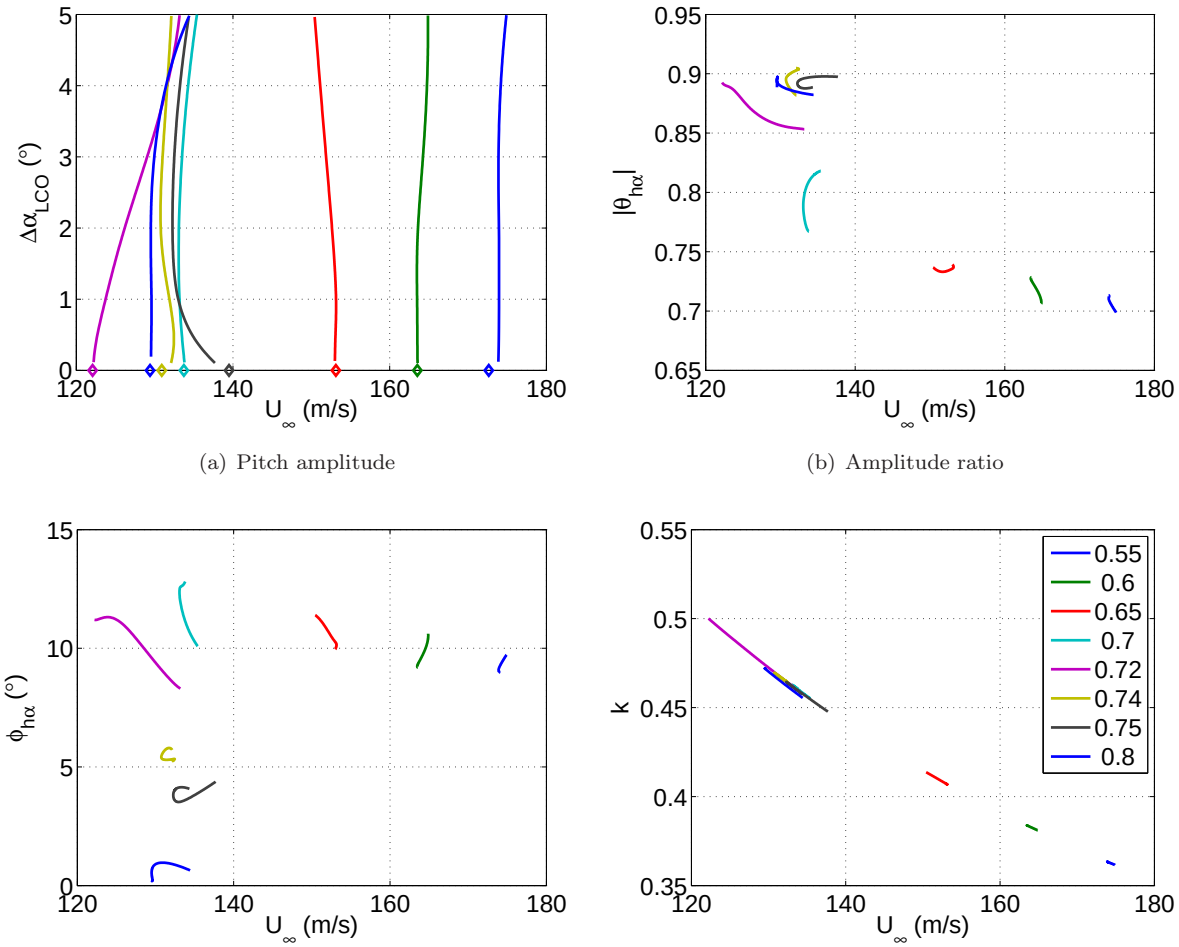

(a) Pitch amplitude

(b) Amplitude ratio

(c) Phase difference

(d) Reduced frequency

Figure 13. LCO mode shape vs freestream velocity for various Mach numbers in inviscid flow

but at the sample locations of the response surface, such that one only sees the effect of the interpolation. Furthermore, slices of the response surface are shown versus pitch amplitude at the flutter mode shape (i.e. $|\theta_{h\alpha}| = 0.8964$, $\phi_{h\alpha} = 4.7966°$ and $k = 0.4424$, red lines) as well as at the mode shape at an LCO amplitude of 5° ($|\theta_{h\alpha}| = 0.8886$, $\phi_{h\alpha} = 4.0775°$ and $k = 0.4576$, green lines). Figure 16 shows that ϕ_{Lh} exhibits a minimum at about 1.5°. From Figure 15(a), at this amplitude, the stability of the LCO changes from unstable to stable (i.e. a saddle-node bifurcation of LCOs occurs[35]). $|\theta_{Lh}|$, $|\theta_{M\alpha}|$ and $\phi_{M\alpha}$ do not show this behaviour at 1.5°, although the phase of the moment changes curvature at an amplitude of 1°. The flutter and $\Delta\alpha_{LCO} = 5°$-mode shapes are very similar, they are only shifted on the ordinate. A direct comparison of the shape of ϕ_{Lh} interpolated at the flutter mode shape and that of the bifurcation diagram is obtained when the freestream velocity is plotted versus the LCO amplitude, see Figure 17(a). Comparing this figure with Figure 16(c) clearly shows that the phase of the lift and the bifurcation diagram exhibit the same shape. In general, it was found that comparing the shape of the sine of ϕ_{Lh} at the flutter- and $\Delta\alpha_{LCO} = 5°$-mode shape is a better measure for the shape of the bifurcation diagram, see Figures 17(a) and 17(b). For this test case ϕ_{Lh} is close to zero and therefore the phase of the lift exhibits the same shape as the sine of this phase. However, when the phase of the lift is not close to zero, the sine of ϕ_{Lh} naturally has a different shape.

The same analysis has been performed for the viscous flow test case. The results in terms of freestream velocity versus LCO amplitude, sine of the phase of the lift interpolated at the flutter mode shape and at the $\Delta\alpha_{LCO} = 5°$-mode shape, are shown in Figure 18. From this figure it is observed that the sine of the phase of the lift and the freestream velocity also exhibit the same shape. Hence, this suggests that when the

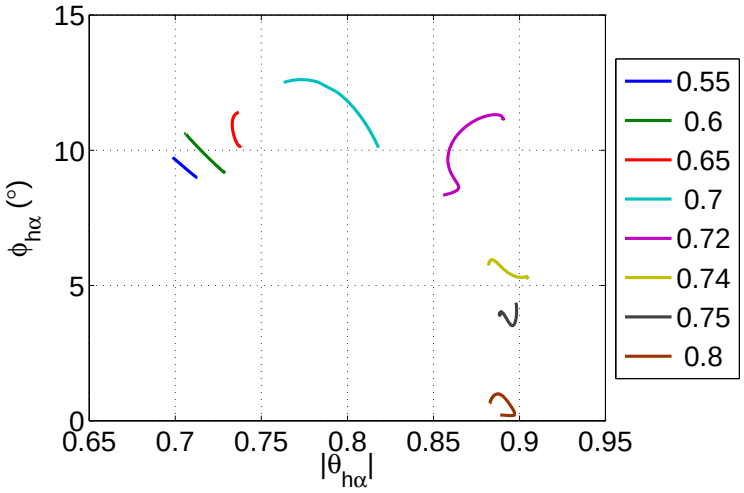

Figure 14. LCO phase difference versus the LCO amplitude ratio for various Mach numbers in inviscid flow

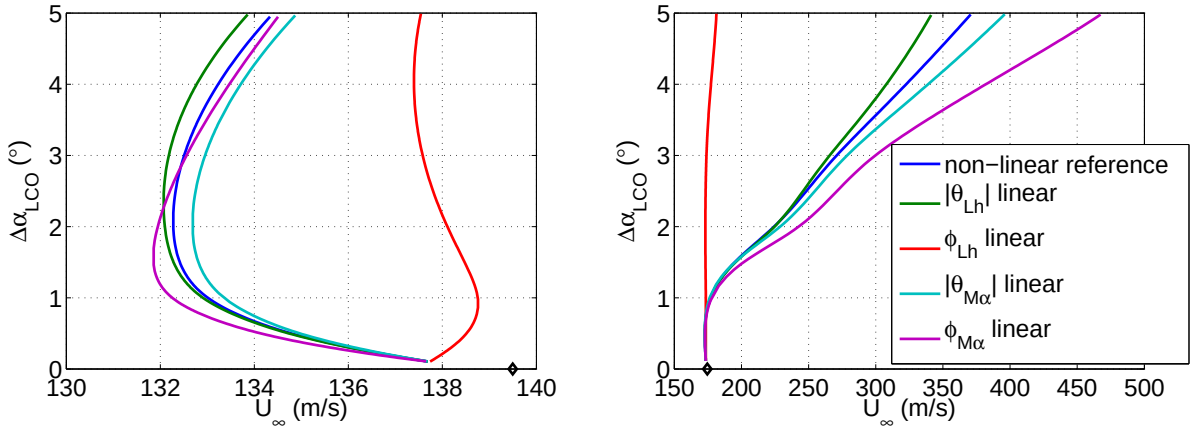

(a) $M_\infty = 0.75$, $\bar{\alpha} = 0°$

(b) $M_\infty = 0.75$, $\bar{\alpha} = 0.7°$, $\mathrm{Re} = 2 \cdot 10^6$

Figure 15. LCO amplitude vs freestream velocity in inviscid flow at $M_\infty = 0.75$, $\bar{\alpha} = 0°$ and in viscous flow at $M_\infty = 0.75$, $\bar{\alpha} = 0.7°$ applying one-at-a-time constant aerodynamic forces

non-linearity in the phase of the lift is responsible for the bifurcation behaviour (i.e. when a constant ϕ_{Lh} results in a significantly different bifurcation behaviour), the shape of the response surface of the sine of the phase of the lift is the same as that of the bifurcation diagram. In case a constant magnitude of the moment $|\theta_{M\alpha}|$ results in a significantly different bifurcation behaviour (e.g. for $M_\infty = 0.8$, $\bar{\alpha} = 0°$ in inviscid flow), the shape of the response surface does not exactly match that of the bifurcation diagram, but the overall trend is the same.

The observations made above are valid for test cases at the nominal structural parameters (see Table 2) and at zero structural damping. However, when the structural frequency ratio is changed, the shape of the bifurcation diagram is not always the same as that of the sine of ϕ_{Lh} at the flutter mode shape. In most cases there is an agreement in shape, but this is not generally true. At $M_\infty = 0.75$, $\bar{\alpha} = 0.7°$ and $\omega_h/\omega_\alpha = 1.20971$ in viscous flow for example, the shape of the rotated bifurcation diagram does not agree with either the phase of the lift nor the sine of the phase of the lift. Although the phase of the lift is the only parameter that results in a completely different bifurcation behaviour when ϕ_{Lh} is constant. However, for the remainder of this section the nominal structural parameters are considered and hence the the observations about the

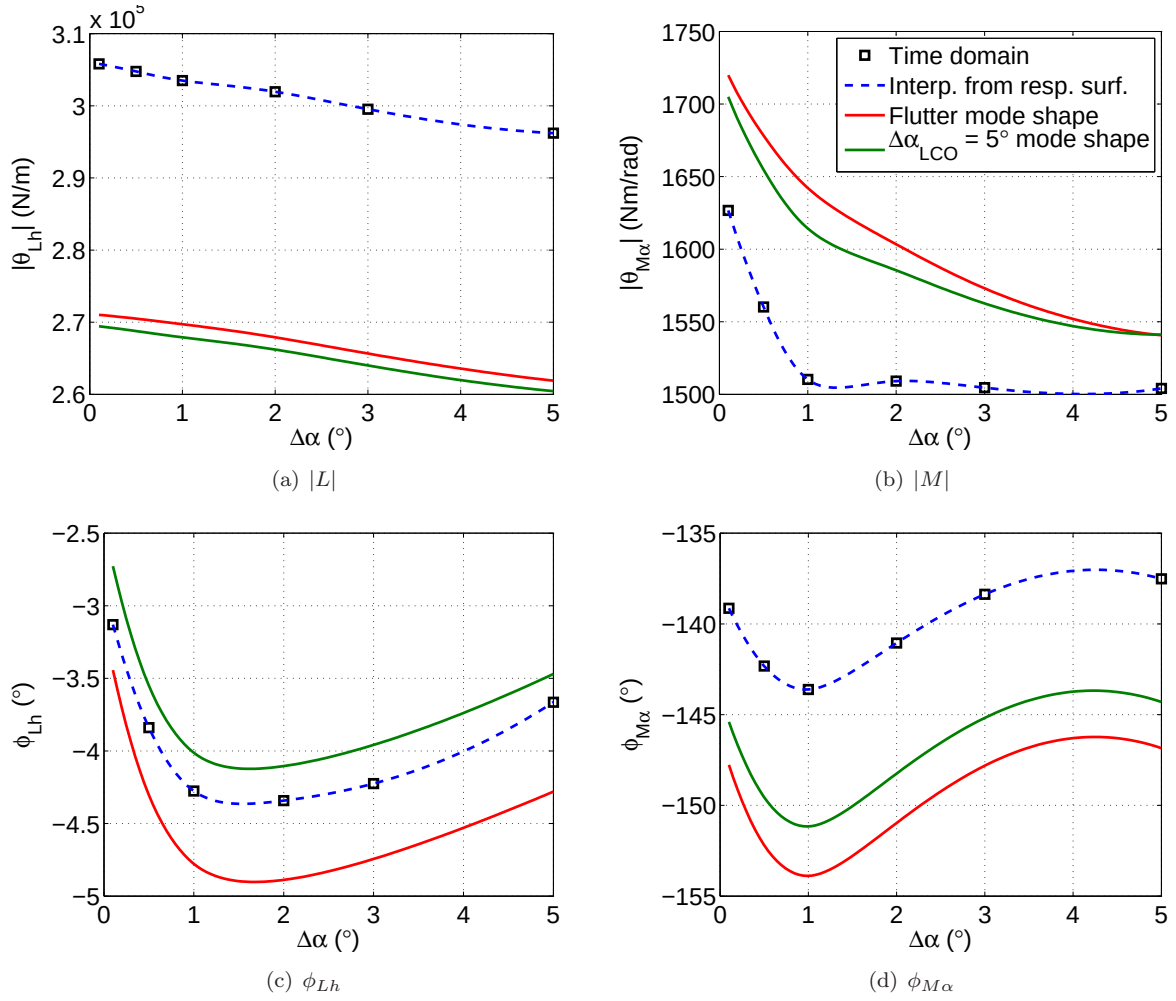

(a) $|L|$ (b) $|M|$

(c) ϕ_{Lh} (d) $\phi_{M\alpha}$

Figure 16. Response surface versus pitch amplitude for Euler simulations at $M_\infty = 0.75$, $\bar{\alpha} = 0°$ at $|\theta_{h\alpha}| = 0.75$, $\phi_{h\alpha} = 5°$ and $k = 0.5$, flutter mode shape and $\Delta\alpha_{LCO} = 5°$-mode shape

bifurcation behaviour and the shape of the response surface at the nominal structural parameters will be used.

Now a link has been established between the bifurcation diagram and the response surface, the response surface can be searched for changes in curvature that might result in other types of bifurcations. If these other types of bifurcations will occur depends on the structural properties. Furthermore, another open question might be answered using the link between the response surface and the bifurcation behaviour; which aerodynamic features are responsible for the form of the response surface? In order to do so, the unsteady local force distributions are considered.

For the inviscid flow case at $M_\infty = 0.75$, $\bar{\alpha} = 0°$ forced motion computations have been performed at the flutter mode shape and frequency, but with various pitch amplitudes ($\Delta\alpha = 0.1°$, $0.5°$, $1.0°$, $2.0°$, $3.0°$, $4.0°$, and $5.0°$). The same phase of the lift versus amplitude was obtained as when using interpolation on the response surface. The local force distribution was assessed to find out why the phase of the lift has this shape. The local magnitude (scaled with the pitch amplitude) and phase angle of the lift distributions are depicted in Figure 19. The phase of the lift is seen to decrease with increasing pitch amplitude, up to an amplitude of $2°$, for larger amplitudes the phase increases again. This decrease can be explained as the typical effect that occurs with increasing pitch amplitude, i.e. the shock peaks decrease in height and spread out when the amplitude increases. This causes a decrease in the area under the local lift distribution. However, for $\Delta\alpha > 2°$ the phase of the lift increases. This increase can be explained from the local phase of the lift distribution as well. For amplitudes of $2°$ and larger there is a shock wave on the lower surface during part

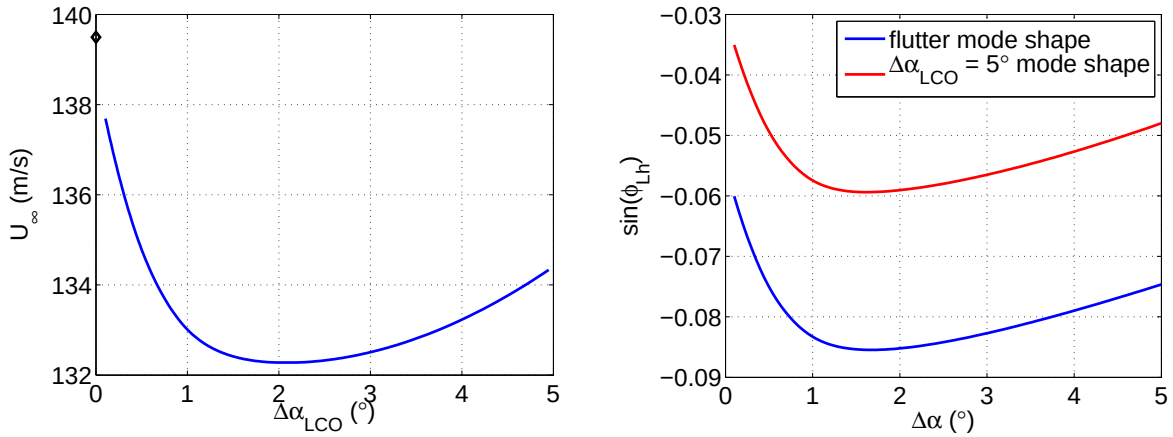

(a) U_∞ vs. $\Delta\alpha_{LCO}$ (b) $\sin(\phi_{Lh})$ vs. $\Delta\alpha$

Figure 17. Freestream velocity versus LCO amplitude and ϕ_{Lh} versus pitch amplitude for Euler simulations at $M_\infty = 0.75$, $\bar{\alpha} = 0°$ at flutter mode shape

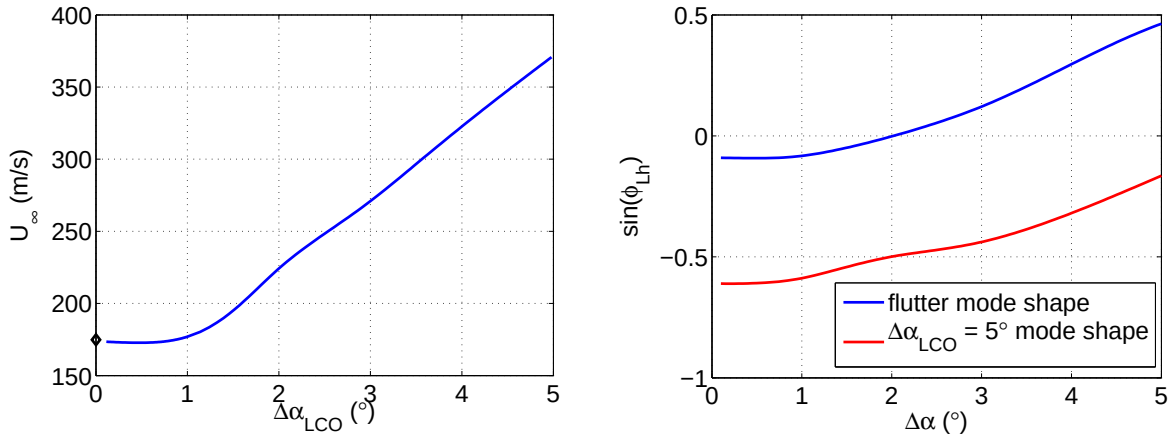

(a) U_∞ vs. $\Delta\alpha_{LCO}$ (b) $\sin(\phi_{Lh})$ vs. $\Delta\alpha$

Figure 18. Freestream velocity versus LCO amplitude and ϕ_{Lh} versus pitch amplitude for RANS simulations at $M_\infty = 0.75$, $\bar{\alpha} = 0.7°$ at flutter mode shape and $\Delta\alpha_{LCO} = 5°$-mode shape

of the oscillation cycle, whereas at small amplitudes there is no shock wave on this surface. This Tijdeman[36] type B (i.e. intermittent) shock motion on the lower surface causes the phase of the lift to increase again. Hence, the shock motion on the lower surface causes the subcritical bifurcation with stable LCOs below the flutter boundary. This is in accordance with the observations of Bendiksen,[30,37] who also found that the change of the shock motion type is responsible for limit-cycle oscillations in inviscid flow.

For the viscous test case at $M_\infty = 0.75$ and $\bar{\alpha} = 0.7°$ it is also observed that the (intermittent) shock motion of the lower surface causes the increase of the phase of the lift, see Figure 20. The Tijdeman[36] type B shock wave motion on the lower surface becomes larger and larger with increasing amplitude, this causes the phase of the lift on the lower surface to become positive over almost the complete surface. Therefore, in this case, the shock motion on the lower surface causes the supercritical bifurcation.

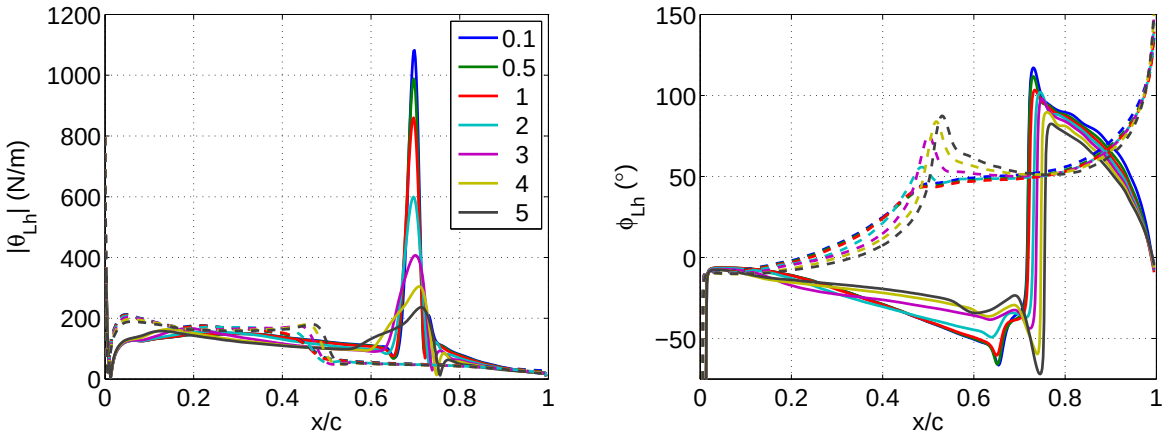

(a) $|\theta_{Lh}|$ vs. x/c (b) ϕ_{Lh} vs. x/c

Figure 19. Local force- and moment distribution for Euler simulations at $M_\infty = 0.75$, $\bar{\alpha} = 0°$ at flutter mode shape

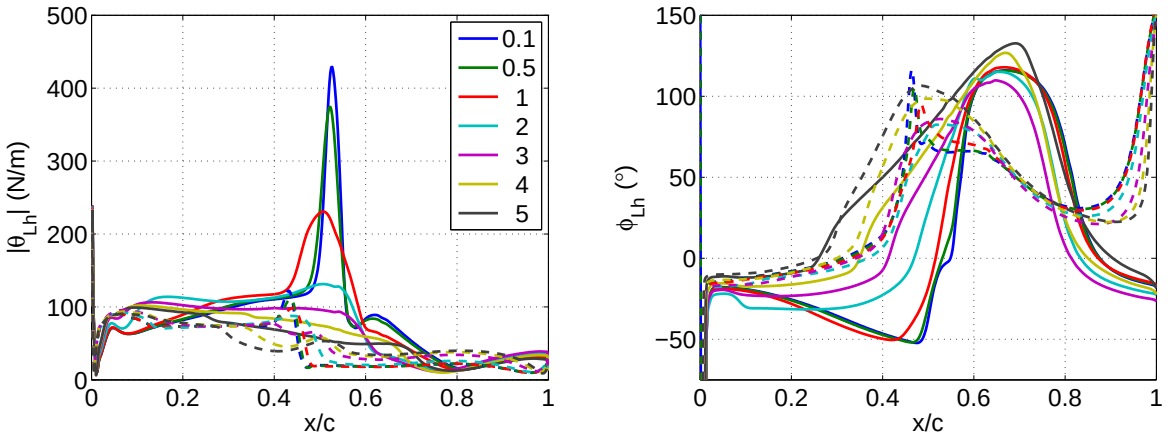

(a) $|\theta_{Lh}|$ vs. x/c (b) ϕ_{Lh} vs. x/c

Figure 20. Local force- and moment distribution for RANS simulations at $M_\infty = 0.75$, $\bar{\alpha} = 0°$ at flutter mode shape

IV. Conclusions

This paper has investigated the bifurcation behaviour of limit-cycle oscillation solutions of a two degree-of-freedom airfoil. A variation of the (linear) structural model parameters has been applied and its effect on the bifurcation behaviour has been studied. The structural frequency ratio and the elastic axis location of the two DoF airfoil system have been varied. Varying the structural frequency ratio showed that even though the bifurcation at the nominal structural frequency ratio is supercritical, a change in structural frequency ratio can make the bifurcation subcritical (or the other way around). Hence, a change in structural stiffness can cause LCOs below the (linear) flutter boundary. Furthermore, it was found that a subcritical bifurcation does not always have to be pitch dominated and the supercritical bifurcation is not always plunge dominated. When the elastic axis was shifted to a location behind the quarter-chord point similar bifurcation behaviour as when the elastic axis is located at the quarter-chord point was observed. However, the slope of the bifurcation curve changed significantly. When the non-linearity is weak, shifting the elastic axis will quickly result in a change of bifurcation type. Overall, it can be concluded that variations in the structural parameters must be

considered when predicting of limit-cycle oscillations, as they significantly affect the bifurcation behaviour (in both strength and type).

The effects of a Mach number variation in inviscid flow on the flutter behaviour and the LCO bifurcation behaviour have also been studied. LCOs were observed even for subsonic Mach numbers, although the non-linearity is much smaller for these Mach numbers than for Mach number near the transonic dip. If LCOs of a certain amplitude, for example 4°, are allowed, the transonic dip can be significantly reduced. It may disappear altogether if LCOs of even larger amplitude are allowed. Subcritical bifurcation behaviour was observed for Mach numbers just below and just above the transonic dip location. At the transonic dip, the bifurcation was supercritical.

Finally, the relation between the aerodynamic forces and the LCO bifurcation behaviour has been studied. The phase of the lift was found to be responsible for the type of bifurcation that occurs for the two DoF airfoil system at its nominal structural parameters. The shape of the rotated bifurcation diagram, i.e. the freestream velocity versus the LCO amplitude, is very similar to that of the sine of the phase of the lift versus oscillation amplitude at the flutter mode shape (and at the $\Delta\alpha_{\mathrm{LCO}} = 5°$-mode shape). Hence, in that case, only a flutter calculation and a few forced motion oscillation simulations at the flutter mode shape would be sufficient to determine the bifurcation behaviour. However, the sine of the phase of the lift does not always have the same shape as the LCO amplitude bifurcation diagram when the structural frequency ratio is varied. Nevertheless, for both transonic flow test cases at the nominal structural parameters it was investigated what causes the shape of the phase of the lift versus oscillation amplitude. For both cases, the shock motion on the lower surface was found to be responsible for the curvature of the phase of the lift and hence for the bifurcation behaviour.

Overall this paper has shown that the limit-cycle oscillations can occur below the flutter boundary predicted from linearised theory. This investigation serves a first step for studies of larger degree-of-freedom systems.

References

[1]van Rooij, A., Nitzsche, J., and Dwight, R., "Energy budget analysis of aeroelastic limit-cycle oscillations," *Journal of Fluids and Structures*, 2016, Accepted for publication.

[2]van Rooij, A., Nitzsche, J., and Dwight, R., "Prediction of aeroelastic limit-cycle oscillations based on harmonic forced motion oscillations," *International Forum on Structural Dynamics and Aeroelasticity (IFASD)*, Saint Petersburg, Russia, June 28-July 2 2015.

[3]van Rooij, A., Nitzsche, J., and Dwight, R., "Prediction of aeroelastic limit-cycle oscillations based on harmonic forced motion oscillations," *AIAA journal*, 2016, Submitted for publication.

[4]Dowell, E., Edwards, J., and Strganac, T., "Nonlinear Aeroelasticity," *Journal of Aircraft*, Vol. 40, No. 5, 2003, pp. 857–874.

[5]Thomas, J., Dowell, E., and Hall, K., "Modeling Viscous Transonic Limit Cycle Oscillation Behavior Using a Harmonic Balance Approach," *43rd AIAA/ASME/ASCE/AHS/ASC Structures, Structural Dynamics, and Materials Conference and Exhibit*, No. AIAA 2002-1414, Duke University, Durham, NC, Denver, CO, USA, April 2002, pp. 1–9.

[6]Kholodar, D., Thomas, J., and Dowell, E., "A Parameter Study of Transonic Airfoil Flutter and Limit Cycle Oscillation Behaviour," *43rd AIAA/ASME/ASCE/AHS/ASC Structures, Structural Dynamics, and Materials Conference and Exhibit*, No. 2002-1211, Denver, CO, USA, April 2002, pp. 1–16.

[7]Kholodar, D., Dowell, E., Thomas, J., and Hall, K., "Limit-Cycle Oscillations of a Typical Airfoil in Transonic Flow," *Journal of Aircraft*, Vol. 41, No. 5, 2004, pp. 1067–1072.

[8]Dowell, E. and Tang, D., "Nonlinear Aeroelasticity and Unsteady Aerodynamics," *AIAA Journal*, Vol. 40, No. 9, September 2002, pp. 1697–1707.

[9]Zhang, W., Wang, B., Ye, Z., and Quan, J., "Efficient Method for Limit Cycle Flutter Analysis by Nonlinear Aerodynamic Reduced-Order Models," *AIAA Journal*, Vol. 50, No. 5, 2012.

[10]Mannarino, A. and Mantegazza, P., "Nonlinear aeroelastic reduced order modeling by recurrent neutral networks," *Journal of Fluids and Structures*, Vol. 48, 2014, pp. 103–121.

[11]Kousen, K. and Bendiksen, O., "Nonlinear aspects of the transonic aeroelastic stability problem," No. 88-2306, 1988, AIAA/ASME/ASCE/AHS 29th Structures, Structural Dynamics and Materials Conference.

[12]Balajewicz, M. and Dowell, E., "Reduced-order modeling of flutter and limit-cycle oscillations using the sparse volterra series," *Journal of Aircraft*, Vol. 49, No. 6, 2012.

[13]Hassig, H., "An Approximate True Damping Solution of the Flutter Equation by Determinant Iteration," *Journal of Aircraft*, Vol. 8, No. 11, 1971, pp. 885–889.

[14]Gerhold, T., Galle, M., Friedrich, O., and Evans, J., "Calculation of Complex Three-Dimensional Configurations employing the DLR TAU-Code." *35th AIAA Aerospace Sciences Meeting & Exhibit*, No. AIAA Paper 97-0167, Reno, NV, USA, January 6-9 1997.

[15]Jameson, A., Schmidt, W., and Turkel, E., "Numerical Solutions of the Euler Equations by Finite Volume Methods Using Runge-Kutta Time-Stepping Schemes," AIAA Paper 1981-1259, June 1981.

[16]Jameson, A., "Time Dependent Calculations Using Multigrid, with Applications to Unsteady Flows Past Airfoils and Wings," *AIAA 10th Computational Fluid Dynamics Conference*, No. AIAA Paper 91-1596, Honolulu, Hawai, USA, June 24-26 1991.

[17]Menter, F., "Two-Equation Eddy-Viscosity Turbulence Models for Engineering Applications," *AIAA Journal*, Vol. 32, No. 8, 1994, pp. 1598–1605.

[18]Schewe, G., Knipfer, A., Mai, H., and Dietz, G., "Experimental and Numerical Investigation of Nonlinear Effects in Transonic Flutter," Internal Report DLR IB 232 - 2002 J 01, Deutsches Zentrum für Luft- und Raumfahrt e.V. (DLR), Institut für Aeroelastik, Göttingen, Germany, 2002.

[19]Schewe, G., Mai, H., and Dietz, G., "Nonlinear effects in transonic flutter with emphasis on manifestations of limit cycle oscillations," *Journal of Fluids and Structures*, Vol. 18, 2003, pp. 3–22.

[20]Dietz, G., Schewe, G., Kiessling, F., and Sinapius, M., "Limit-cylce-oscillation experiments at a transport aircraft wing model," *International Forum on Structural Dynamics and Aeroelasticity (IFASD)*, Deutsches Zentrum für Luft- und Raumfahrt, Institut für Aeroelastik, Amsterdam, The Netherlands, June 2003.

[21]Dietz, G., Schewe, G., and Mai, H., "Experiments on heave/pitch limit-cycle oscillations of a supercritical airfoil close to the transonic dip," *Journal of Fluids and Structures*, Vol. 19, 2004, pp. 1–16.

[22]Dietz, G., Schewe, G., and Mai, H., "Amplification and amplitude limitation of heave/pitch limit-cycle oscillations close to the transonic dip," *Journal of Fluids and Structures*, Vol. 22, 2006, pp. 505–527.

[23]Weber, S., Jones, K., Ekaterinaris, J., and Platzer, M., "Transonic flutter computations for a 2D supercritical wing," *37th AIAA/ASME/ASCE/AHS/ASC Structures, Structural Dynamics, and Materials Conference and Exhibit*, No. A99-16647, Naval Postgraduate School, Monterey, CA, Reno, NV, USA, January 1999.

[24]Castro, B., Jones, K., Ekaterinaris, J., and Platzer, M., "Analysis of the effect of porous wall interference on transonic airfoil flutter," *31st AIAA Fluid Dynamics Conference & Exhibit*, Naval Postgraduate School, Monterey, CA, Anaheim, CA, USA, June 2001.

[25]Tang, L., Bartels, R., Chen, P., and Liu, D., "Numerical investigation of transonic limit cycle oscillations of a two-dimensional supercritical wing," *Journal of Fluids and Structures*, Vol. 17, 2003, pp. 29–41.

[26]Wang, B. and Zha, G.-C., "Numerical simulation of transonic limit cycle oscillations using high-order low-diffusion schemes," *Journal of Fluids and Structures*, Vol. 26, 2010, pp. 579–601.

[27]Thomas, J., Dowell, E., and Hall, K., "Modeling Limit Cycle Oscillations for an NLR 7301 Airfoil Aeroelastic Configuration Including Correlation with Experiment," *44th AIAA/ASME/ASCE/AHS/ASC Structures, Structural Dynamics, and Materials Conference and Exhibit*, No. AIAA 2003-1429, Duke University, Durham, NC, Norfolk, VA, April 2003, pp. 1–9.

[28]Weber, S., Jones, K., Ekaterinaris, J., and Platzer, M., "Transonic flutter computations for the NLR 7301 supercritical airfoil," *Aerospace Science and Technology*, Vol. 5, 2001, pp. 293–304.

[29]Tang, L., Bartels, R., Chen, P., and Liu, D., "Simulation of transonic limit cycle oscillations using a cfd time-marching method," *42nd AIAA/ASME/ASCE/AHS/ASC Structures, Structural Dynamics, and Materials Conference and Exhibit*, No. AIAA 2001-1290, Seattle, WA, April 2001, pp. 1–9.

[30]Bendiksen, O., "Transonic Limit Cycle Flutter/LCO," *45th AIAA/ASME/ASCE/AHS/ASC Structures, Structural Dynamics, and Materials Conference*, No. AIAA 2004-1694, Univerisity of California, Los Angelos, Palm Springs, California, April 2004, pp. 1–17.

[31]Saitoh, K. and Kheirandish, H., "Numerical Simulation of Small Amplitude LCO for NLR-7301 Profile," *International Forum on Structural Dynamics and Aeroelasticity (IFASD)*, Stockholm, Sweden, June 2007.

[32]Saitoh, K., Voss, R., and Kheirandish, H., "Numerical Study of Nonlinearity of Unsteady Aerodynamics for NLR7301 Profile," *International Forum on Structural Dynamics and Aeroelasticity (IFASD)*, Munich, Germany, June/July 2005.

[33]Yang, S., Zhang, Z., Liu, F., Luo, S., Tasi, H.-M., and Schuster, D., "Time-Domain Aeroelastic Simulation by a Coupled Euler and Integral Boundary-Layer Method," *22nd Applied Aerodynamics Conference and Exhibit*, Providence, RI, USA, August 2004, pp. 1–12.

[34]Hall, K., Thomas, J., and Dowell, E., "Proper Orthogonal Decomposition Technique for Transonic Unsteady Aerodynamic Flows," *AIAA Journal*, Vol. 38, No. 10, 2000, pp. 1853–1862.

[35]Gros, C., "Bifurcations and Choas in Dynamical Systems," Tech. rep., Goethe Universität Frankfurt am Main, 2014, Lecture notes course Self-Organization: Theory and Simulation.

[36]Tijdeman, H., *Investigations of the transonic flow around oscillation airfoils*, Ph.D. thesis, Technische Hogeschool Delft, 1977.

[37]Bendiksen, O., "Influence of Shocks on Transonic Flutter of Flexible Wings," *50th AIAA/ASME/ASCE/AHS/ASC Structures, Structural Dynamics, and Materials Conference*, No. AIAA 2009-2313, University of California, Los Angeles, Palm Springs, CA, USA, May 2009.